AD NUMBER

AD841048

LIMITATION CHANGES

TO:

Approved for public release; distribution is unlimited. Document partially illegible.

FROM:

Distribution authorized to U.S. Gov't. agencies and their contractors; Critical Technology; SEP 1968. Other requests shall be referred to Air Force Technical Application Center, Washington, DC. This document contains export-controlled technical data.

AUTHORITY

radc, usaf ltr, 17 sep 1971

RADC-TR- 68-395
September 1968

C-BAND PHASED ARRAY CROSSED-FIELD AMPLIFIER DEVELOPMENT

R. Bitzer
A. Wilczek

Contractor: S.F.D. Laboratories
Contract No. F30602-68-C-0055
Effective Date of Contract: 24 July 1967
Contract Expiration Date: 15 December 1968
Amount of Contract: $239,750.00
Program Code No. 7E30

Principal Investigator: Andrew Wilczek
Phone: 201-6870290

Project Engineer: Dirk T. Bussey
Phone: 315 330-3686

Sponsored By
Advanced Research Projects Agency
ARPA Order No. 136
Amendment No. 15

Rome Air Development Center
Air Force Systems Command
Griffiss Air Force Base, New York

C-BAND PHASED ARRAY CROSSED-FIELD AMPLIFIER DEVELOPMENT

R. Bitzer
A. Wilczek
SFD Laboratories

This research was supported by the Advanced Research Projects Agency of the Department of Defense and was monitored by D. K. Bussey RADC (EMATE), GAFB, N.Y. 13440.

BLANK PAGE

ABSTRACT

This program has two main objectives. The first is to demonstrate the feasibility of an RF turn-on, RF turn-off, reentrant stream crossed-field amplifier. The reliability of RF turn-on has previously been demonstrated and during this reporting period, RF turn-off has been demonstrated with only dc voltages applied to the amplifier.

The second objective of this program is to increase the output capability previously demonstrated, under Contract AF 30(602)-4082, by a factor of two. During this period a hot test vehicle has been successfully assembled and the matching transitions have been developed.

TABLE OF CONTENTS

LIST OF ILLUSTRATIONS

1.0 INTRODUCTION

This program effort has two main objectives. The first objective (Contract Line Item A001) is to demonstrate the feasibility of a RF turn-on, RF turn-off, reentrant stream crossed-field amplifier to minimize or eliminate modulation requirements. The second objective of this program (Contract Line Item A002) is to increase the power output capability previously demonstrated, on Contract AF 30(602)-4082, by a factor of two.

This program is a continuation of ARPA sponsored work begun on Contract AF 30(602)-4082. Under that contract, the SFD-237 was developed and operated at a peak power of 1 Mw and an average power of 10 kw. The vehicle incorporated RF turn-on, with RF turn-off accomplished through the use of a control electrode. The RF turn-on experiments performed during the last reporting period demonstrated the feasibility of using a simulated dc operation. To date RF turn-off has been demonstrated reliably with only dc voltages applied to the tube. The spectral performance, pulse burst operation at very high repetition frequencies, and dynamic operating range have also been investigated and found to be very encouraging.

During the period covered by this report, matching techniques have been developed for the high power amplifier. The techniques were developed using a cold test version of the amplifier anode on which the circuit configuration could be easily altered. The resulting information was successfully applied to a hot test vehicle. The matching transitions thus obtained provided very good coupling to the slow wave circuit with the capability of operation at the high peak and average powers required. The anode assembly has been completed for the first hot test vehicle.

The cathode structure is in the process of being constructed. Some delays have been encountered in the assembly of the cathode structure. Porous materials and defective brazes have resulted in a number of "leaky" structures. The difficulties have been partially corrected

and assembly will continue.

The magnetic field pattern has been thoroughly examined and found to be quite uniform over the interaction area.

2.0 SELF-TURN OFF

In the preceding report (RADC-TR-68-122, AD 830 464), the operation of a dc operated crossed-field amplifier with RF turn on and RF turn off was reported. The RF turn off was accomplished by applying a bias voltage between the bias electrode and cathode. This bias voltage was in the form of a long voltage pulse which overlapped the RF pulse and thereby simulated a dc bias voltage. This same amplifier has now been operated with only dc voltages applied, thereby eliminating the need for a pulse modulator.

The connection of the amplifier and its dc power supply for this type of operation is shown schematically in Figure 1. The anode and cathode are connected across the principal energy storage system of the dc power supply while the bias electrode is connected across part of that voltage. The mid-point of voltage in our present experiments is a convenient value to apply to the bias electrode, but it is expected that subsequent experiments and designs will permit the application of lower cathode-to-bias electrode voltage to achieve the same result.

The technique for operating the self-modulated amplifier under these conditions is simply to apply full operating voltage and full bias electrode voltage before applying RF drive. Upon the application of RF drive normal amplification and self-modulation occurs. Figure 2 shows the envelope of the RF drive pulse being delivered to the amplifier (lower trace) on a time base of 1 μsec per cm. The envelope of the amplifier RF output is shown as the upper trace. The operating conditions shown for this oscillogram and those to follow are approximately:

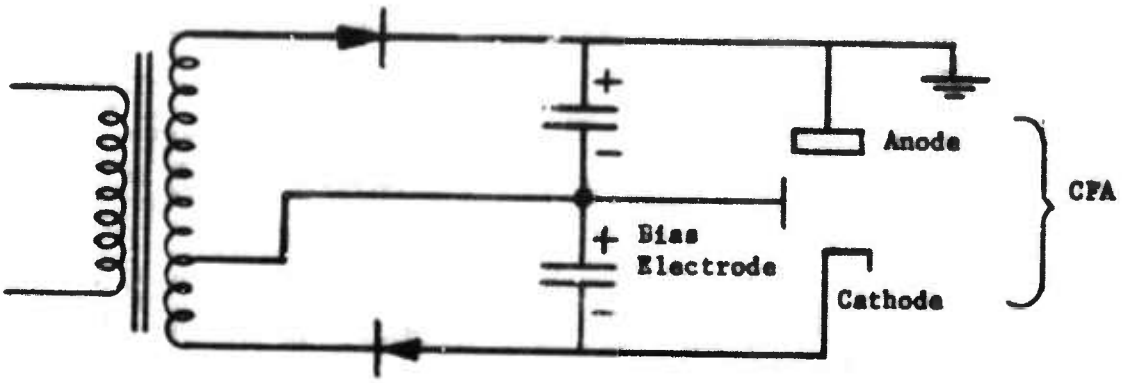

FIGURE 1 SCHEMATIC OF BIAS ELECTRODE CIRCUIT CONNECTION IN SELF-MODULATED AMPLIFIER

This simplified circuit diagram shows the connection of a self-modulated CFA to the dc power supply. The bias electrode operates from a portion of the transformer secondary. Our present experiments utilize a transformer center top giving a bias voltage equal to half anode-cathode voltage. This value is expected to become lower as work with this technique proceeds.

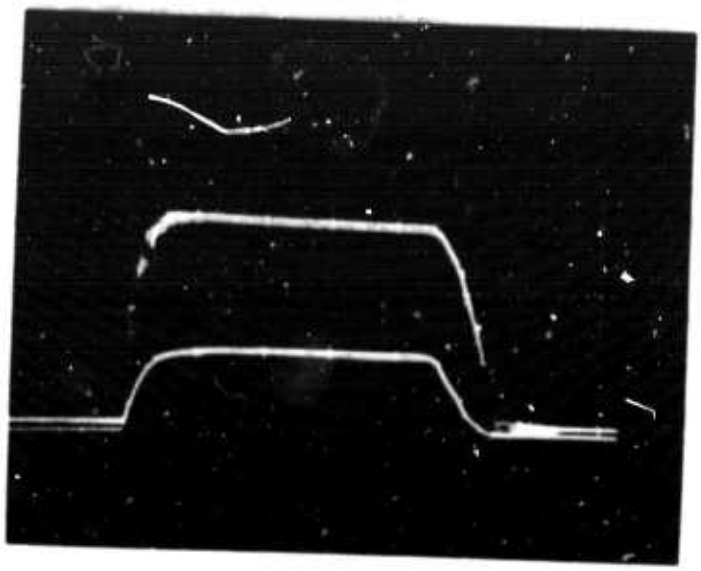

FIGURE 2 RF ENVELOPE OF AMPLIFIED PULSE UNDER SELF-MODULATION CONDITIONS

The lower trace shows the RF envelope of the drive pulse applied to the amplifier operating solely from a dc source. The time scale is 1 μsec/cm. The upper trace is the envelope of the RF output at 500 kw peak. The leading edge ripples are video effects produced by the external circuits. Note that the RF output follows the RF input as it rises and falls. The amplifier is non-linear but has dynamic range. Gain under these conditions is more than 8 db.

Duty Factor	0.001
Pulse Width	5 μsec
PRF	200 pulses per second
Operating Voltage	21.5 kv dc
Bias Voltage	11 kv dc
Peak Output Power	500 kw
Gain	8 to 10 db

Both RF input and RF output detectors are broad banded so that spurious outputs, if present, would be detected.

Figure 3 shows the RF envelope of the amplified output pulse (upper trace) and the cathode current pulse (lower trace). The close similarity of the shape of these pulses is apparent. Note particularly that the cathode current and the RF output cease at the same time. This is a more positive indicator that the amplifier has turned off than the cessation of the RF output alone. It is possible for amplifiers of this type to continue to operate and draw cathode current without necessarily generating, in the output waveguide system, an easily measurable amount of power. This can occur through the excitation of spurious modes on the internal structure which are not coupled to the output system. The absence of cathode current, however, indicates the absence of this type of interaction when the RF drive is removed.

Figure 4 shows the three parameters of input, output and cathode current on the same display.

2.1 Self-modulation Performance

After the demonstration of reliable self-modulated operation, the performance of the amplifier under these conditions was examined in a number of ways for possible limitations. First, the RF drive signal was turned over the entire 5.4 GHz to 5.9 GHz frequency range of the SFD-237 and the self-modulation was shown to be completely insensitive to frequency. Any variations in performance which were

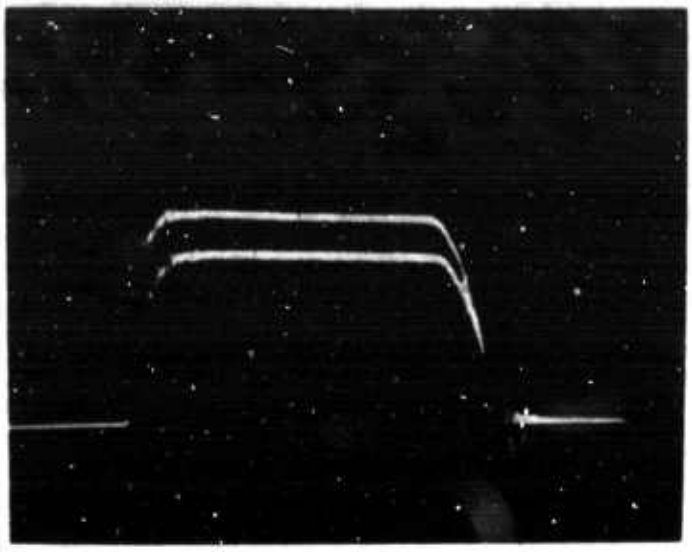

FIGURE 3 RF ENVELOPE AND CATHODE CURRENT PULSE UNDER SELF-MODULATION CONDITIONS

The upper trace is the RF output at 500 kw. The lower trace is the cathode current of about 60 amps peak. The ripples on the leading edges are video effects caused by external circuitry. Power output and current appear directly proportional. The cessation of cathode current at the end of the RF pulse is the most direct evidence that the amplifier has turned off and is no longer operating in any unusual mode. The RF detector used is broad band to show spurious output if it occurred.

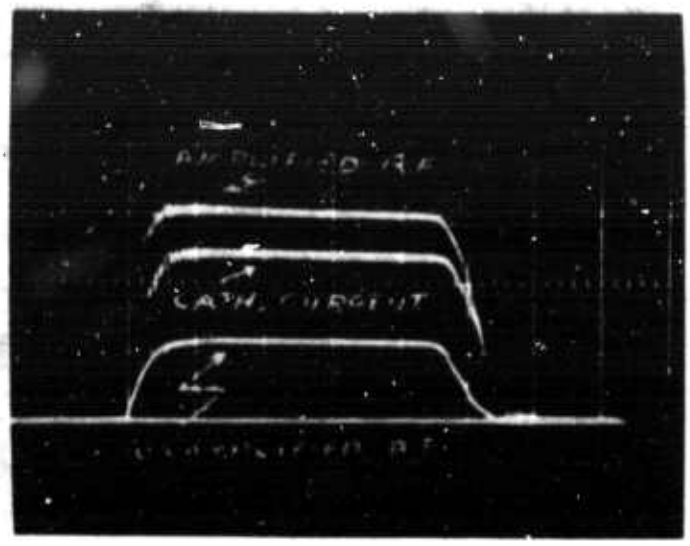

FIGURE 4 RF INPUT, RF OUTPUT AND CATHODE CURRENT PULSES UNDER SELF-MODULATION CONDITIONS

This photograph displays the three most pertinent parameters together during self-modulated operation at 500 kw output. Leading edge ripples in the current and RF output pulses are caused by power supply inductance. This produces a current ripple which then produces a ripple in the RF output. The absence of current following the end of the RF drive pulse is evidence of the turn off of the tube.

observed were accountable from sources other than the self-modulation technique.

Second, the RF drive level was varied over a range of about 7 db without producing instability in the output of the amplifier. The variation in drive ranged from 3 db below the normal level of 50 kw to 4 db above it. The amplifier as expected was not linear over this variation in drive amplitude. For each db variation in RF drive level, the output power changed by approximately 0.7 db.

Third, the voltage level applied to the amplifier was varied in order to produce cathode current variations. The amplifier was stable for all voltage levels from the Hartree voltage out to that which produced maximum available current (the maximum current boundary). This corresponded to peak cathode current levels of approximately 100 amperes. This experiment verified that the self-modulation effect is not voltage sensitive and could be used for a range of power output and gain levels.

Fourth, the starting jitter was examined on this first experimental vehicle to see if the existence of voltage on the bias electrode produced unusual behavior during starting. The jitter was found to be equal to or less than 4 nsec which we feel, especially for this first vehicle, to be quite an acceptable value.

2.2 Spectral Data

Following these experiments the relative purity of amplification was examined to determine whether any basic sacrifice in amplifier performance was required in order to achieve the self-modulation. The pulse spectrum of the RF drive source was photographed from a spectrum analyzer display with a spectrum width of approximately 300 kHz per division and a vertical sensitivity of 10 db per division (a logarithmic display). The driver spectrum is shown in Figure 5. The asymmetry of the driver spectrum is caused by frequency modulation from the finite rise and fall time of the voltage pulse being applied

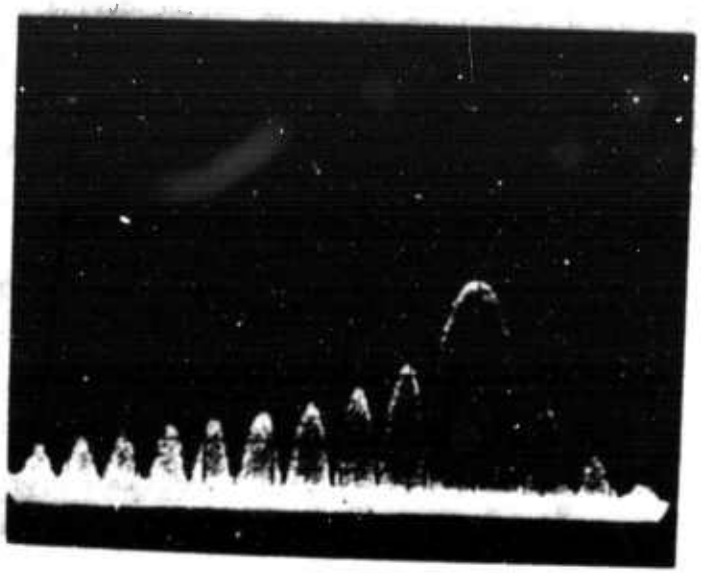

FIGURE 5 SPECTRUM OF RF INPUT PULSE TO SELF-MODULATED AMPLIFIER

A drive pulse of 5 μsec is used. The spectrum shown here is on a logarithmic display with a vertical sensitivity of 10 db/cm. The drive pulse spectrum has better than 10 db side lobe ratio. The asymmetry of the spectrum is caused by frequency modulation of the magnetron used to generate the pulse. The spectrum is distorted from the more well-known magnetron spectrum shape because of the logarithmic display. The spectrum width is approximately 300 kHz/cm.

to the driver magnetron and the pushing figure of that magnetron. Nevertheless, the drive pulse has a 10 db or better side lobe ratio. Figure 6 shows the pulse spectrum of the amplified RF output. As far as can be discerned from these photographs there is no spectrum distortion produced by the self-modulation process.

Broad band spectrum data were also obtained to examine the possible generation of unwanted spurious output by the self-modulation process. These broad band data were obtained in several different ways. The measurements were made using a Hewlett Package 8551B spectrum analyzer and a Hewlett Packard 8441A preselector. The differences in the data to be presented are the result of either the selection of different spectrum widths or the selection of different IF bandwidths. The 8551B analyzer has an "automatic" IF bandwidth selector through which the IF bandwidth is determined by the sweep speed and spectrum width which have been selected. The IF bandwidth may also be selected at fixed values such as 100 kHz or 1 MHz. According to the manufacturer's instructions, the IF bandwidth which the analyzer would select on "automatic" in Figures 7 and 8 is 100 kHz.

The amplifier was operated at 5.6 GHz and a number of spectra were photographed. Figure 7A shows the spectrum of the RF drive pulse to the amplifier displayed over 1 GHz. The spectrum width is 100 MHz/cm and the vertical sensitivity is 10 db/cm. This spectrum would reveal the generation of any spurious power by the RF drive. Figure 7B shows the spectrum of the RF output from the amplifier under the same analyzer conditions. The IF bandwidth for both Figures 7A and 7B is "automatic" and is selected by the analyzer according to the combination of spectrum width (1 GHz) and sweep speed (4.5 sec/cm) which was used for this display.

Figures 8A and 8B are similar spectra except over a spectrum width of 2 GHz also with the IF bandwidth on "automatic". For this display the sweep speed was selected at 7.5 sec/cm.

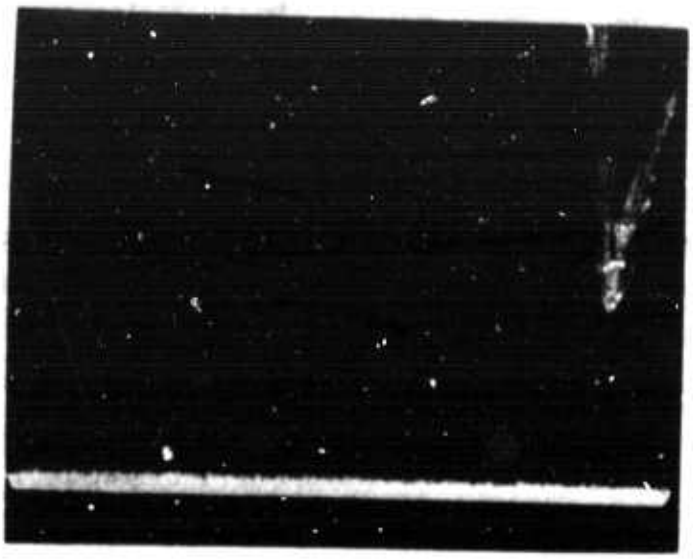

FIGURE 6 SPECTRUM OF RF OUTPUT PULSE FROM SELF-MODULATED AMPLIFIER

This spectrum photograph was made with the same analyzer settings as used in Figure 5. A comparison of the two figures will show the gain of the amplifier to be 8 db to 10 db. Note that the side lobe ratio of the spectrum is still 10 db or more and that the many side lobes visible are still clearly defined. In both figures there is an amplitude decay of about 22 db from the main lobe to the left hand edge of the display. The amplification produces no apparent spectrum distortion.

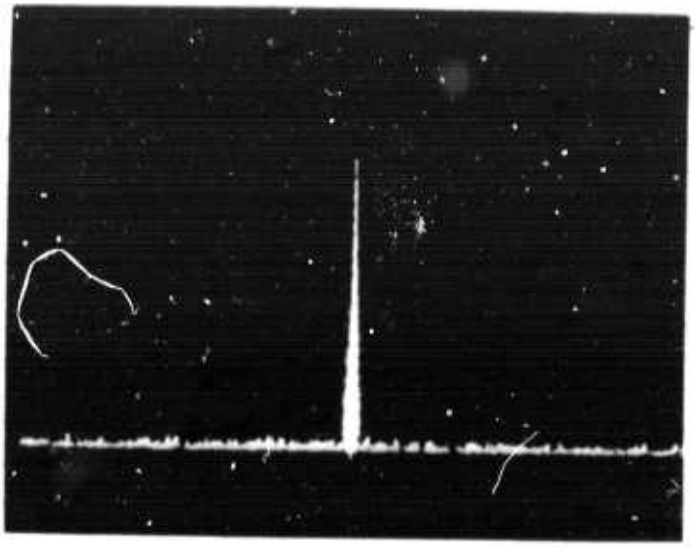

A. 1 GHz spectrum of RF drive pulse

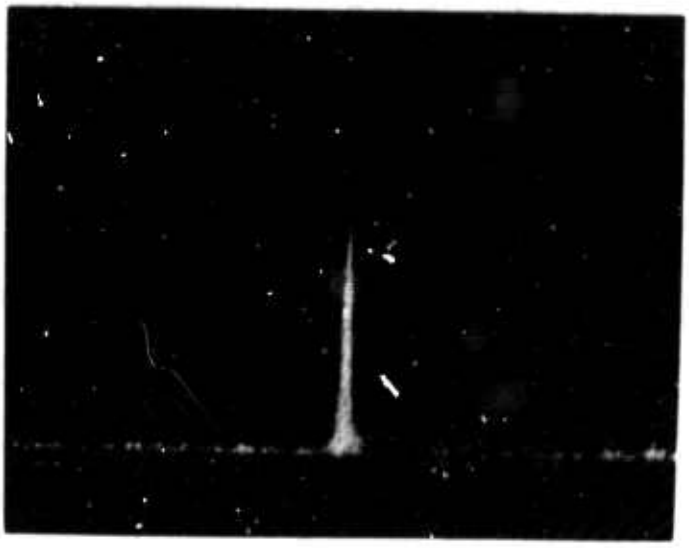

B. 1 GHz spectrum of RF output pulse from self-modulated amplifier

FIGURE 7 1 GHz SPECTRA USING 100 kHz BANDWIDTH

The spectrum analyzer using 100 kHz bandwidth shows spurious output more than 40 db below carrier. Self-modulation produces no spurious outputs, indicating the turn off is complete.

A. 2 GHz spectrum of RF drive pulse

B. 2 GHz spectrum of RF output pulse from self-modulated amplifier

FIGURE 8 2 GHz SPECTRA USING 100 kHz BANDWIDTH

The broad spectrum width used here reduces the intensity of the carrier on the spectrum display. The carrier peak in the top picture is 50 db above the base line; in the bottom picture about 58 db above the base line. Spurious outputs using 100 kHz bandwidth are 45 db or more below the carrier.

A third spectrum display was obtained by selecting a fixed 1 MHz IF bandwidth and a spectrum width of 2 GHz. Figures 9A and 9B show the spectra of the RF drive and RF output respectively from the amplifier. The sweep speed here is also 7.5 sec/cm. From this value it follows that the background spurious output power in Figure 9 would be approximately 10 db higher because the bandwidth of integration in the analyzer is 10 db higher. Even with a 1 MHz IF bandwidth, however, the spurious output is clearly more than 30 db below the signal over the 2 GHz spectrum width.

These results show that no degradation in spectral output is caused by the introduction of the bias electrode.

2.3 Pulse Burst Operation

Since one of the principal advantages of completely self-modulated operation over control electrode operation would manifest itself in conditions of either very high pulse repetition frequency (PRF) operation or under conditions of variable pulse width or interpulse interval, some experiments were conducted to explore any possible limitations of self-modulation in this regard. The design of the experiments was limited in its complexity by available test equipment, but the results demonstrate clearly that self-modulation is indeed applicable to high PRF systems and will operate quite successfully with variable interpulse intervals. To show this the amplifier was driven by a group of three pulses with an interpulse spacing which was variable from a few microseconds upward. Each of the three pulses was approximately 2 μsec long and the three-pulse group was repeated at a rate of 100 groups per second. In this particular demonstration, the driver magnetron was operated from a hard tube modulator. Shown in Figure 10 are the detected RF envelopes of the amplified three-pulse group. In this photograph the interpulse period is approximately 15 μsec. During the experiment the interpulse interval could be manually varied at random with no ill effect.

A. 2 GHz spectrum of RF drive pulse

B. 2 GHz spectrum of RF output pulse from self-modulated amplifier

FIGURE 9 2 GHz SPECTRA USING 1 MHz BANDWIDTH

These broad band spectra were made using a 1 MHz bandwidth. Spurious outputs now appear to be about 35 db below the carrier reflecting the 10 db increase in IF bandwidth used here. Figures 8A and 8B were made using a 100 kHz bandwidth and showed 45 db spurious outputs. Self-modulation produces no spurious outputs, indicating that turn off is complete.

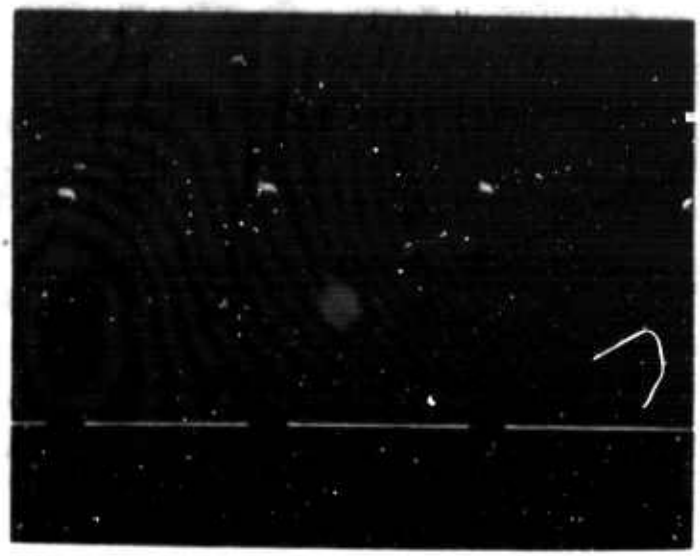

FIGURE 10 RF ENVELOPE OF A THREE-PULSE BURST USING SELF-MODULATED AMPLIFIER

The most difficult modulation problem ordinarily arises with pulse burst operation. This simple illustration of a three-pulse burst shows that a self-modulated amplifier can satisfy these requirements. Three 2 μsec pulses are separated by about 15 μsec each, indicating an intra-burst repetition rate of 65 kHz. The pulses have clean and distinct leading and trailing edges.

In an effort to simulate as high an intra-burst repetition rate as possible, the interpulse spacing of the three-pulse burst was reduced to the limit of the test equipment, about 1.5 μsec. Under these conditions some inadequacies of the test equipment became evident. The RF drive source in Figure 11 is generating the pulse train shown on the bottom trace at 1 μsec/cm. The pulse shapes unfortunately are distorted by voltage droop on the energy storage capacity of the hard tube modulator during the burst. This droop produces both the amplitude change and the pulse shape change. The self-modulated amplifier output in the top trace, however, accurately reproduces both the amplitude change and the pulse shape change. Here the self-modulation process shows itself capable of 300 kHz intra-burst repetition rates. The lower intensity of the amplifier output trace is attributable to the higher writing speed of the oscilloscope under these conditions. The amplifier starts and stops reliably.

2.4 Feedthrough

In addition to making possible the self-modulation process itself, the bias electrode could, if required, be given an additional positive voltage pulse which could prevent the amplifier from turning on at all in order to permit the feedthrough of RF drive power. This type of operation would be quite impossible with linear format distributed emission amplifiers. There appears, therefore, to be no application of which we are aware for which the self-modulation process for a reentrant tube cannot be adapted to advantage.

2.5 Efficiency

What then is the price which must be paid for this successful self-modulation process? The principal area in which overall performance appears to be different from that of the usual SFD-237 is in overall efficiency. In the self-modulated amplifier with a bias electrode, its efficiency has to be redefined to account for some power

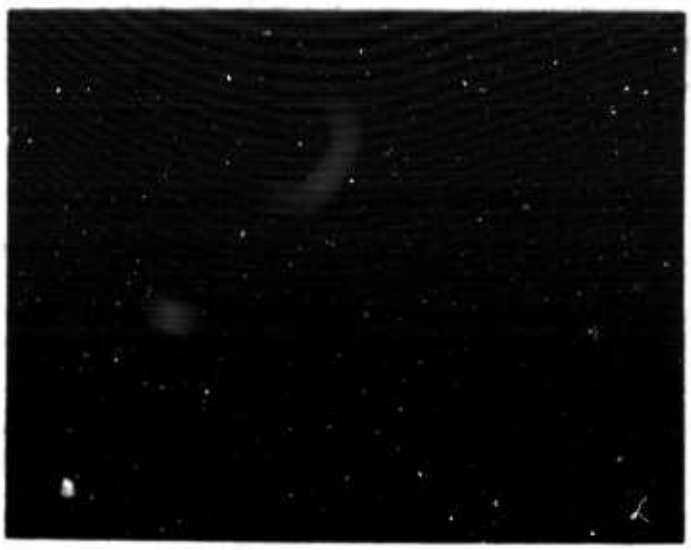

FIGURE 11 RF ENVELOPE OF DRIVE PULSE (LOWER TRACE) AND OUTPUT PULSE (UPPER TRACE) FOR A THREE PULSE BURST FROM SELF-MODULATED AMPLIFIER

These pulses, on a 1 μsec/cm time base, show the capability of the self-modulation process to amplify with 300 kHz repetition rates. The amplitude and pulse shape changes of the RF drive pulse, produced by a capacitor's voltage droop, are reproduced accurately by the CFA. Differences in trace intensities are caused by differences in oscilloscope writing speed.

which is consumed by the bias electrode itself. Since the bias electrode operates at a potential positive with respect to cathode, it becomes a collector of current during the pulse. There are then two components of collected current, the bias electrode current and the anode current, which make up the bulk of power lost in the amplifier (the remainder of which is cathode back bombardment power and circuit losses). One can define an anode efficiency, η_a, as

$$\eta_a = \frac{P_o}{E_{dc} i_a}$$

where P_o is the peak output power
E_{dc} is the anode-cathode voltage
i_a is the peak anode current

An overall efficiency, η_o, can be defined as

$$\eta_o = \frac{P_o}{E_{dc} i_a + E_{be} i_{be}}$$

where i_{be} is the peak bias electrode current
E_{be} is the bias electrode voltage

(Still another overall efficiency can be defined by using total cathode current and anode-cathode voltage. This yields the lowest efficiency value but is slightly pessimistic.)

Observations on the first experimental vehicle indicate an anode efficiency of approximately 38% and an overall efficiency of approximately 35%. The deviation of these values from the norm of 50% for the SFD-237 is not believed to be an accurate gauge of the decrease in efficiency resulting from the self-turn off process. The particular experimental vehicle used did not operate as a normal control electrode tube, at full 50% efficiency and could be considered below par in that respect. It is believed that the reduced efficiency is a result of a

slight difference in the cathode structure used for control electrode operation. A control experiment was performed by rebuilding the test vehicle as a control electrode tube. The efficiency indeed returned to the normal values. Further, visual observations of those vehicles used in the self-turn off experiments also indicate that the loss in efficiency may be due to perturbations that do not exist or are considerably reduced in a control electrode tube. In future experiments, we will attempt to reproduce the control electrode cathode structure in the self-turn off test vehicles to confirm these observations. It is expected that subsequent experiments, particularly those leading to the operation of the bias electrode at lower voltages, will serve to increase the overall efficiency of the amplifier so that it will be in the vicinity of 45%. It is presently felt that the self-modulation process will not interfere with the achievement of what is considered normal anode efficiency of 50% or greater, and that the power lost to the bias electrode can be made small enough to yield such an overall efficiency as 45%.

2.6 Average Power

The maintenance of the anode efficiency at "normal" 50% or higher levels is important in the additional sense that the achievement of very high average power levels with this self-modulation process imposes no greater burden in terms of dissipation on the slow wave circuit than did control electrode operation. The bias electrode is a collector of electrons and also must be designed with a dissipation capability. It is presently felt that the dissipation capability of the bias electrode can be more readily increased, if necessary, than can the capability of the slow wave circuit because of the fewer boundary conditions which the bias electrode imposes on the problem. It remains to be seen, however, if problems will in fact arise in this area. The limits of dissipation capability, unfortunately, could not be examined in the current experiments because a portion of our test

equipment setup was limited in duty factor to approximately 0.001. Experiments will be conducted in the near future, however, hopefully at duty factors up to 0.01.

2.7 Other Experiments

Based upon the results which had been obtained, the next experiments were designed to test our understanding of the mechanism of the bias technique. The geometry of the bias electrode in the next experiment was designed to exaggerate the conditions of the previously successful experiments. It was anticipated that the bias voltage for self-turn off would be reduced and that the RF drive power would have to be increased. It was also anticipated that the bias current would increase because of the new geometry, but the increased RF drive power would partially compensate, so that the actual bias current would be nearly the same as that obtained in the first successful demonstration.

The results of this experiment did show that self-turn off was accomplished at lower bias voltage and that a higher drive power was necessary; however it was also found that the higher drive power did not reduce the bias current significantly. The net result was that self-turn off was accomplished with reduced bias voltage, but the amplifier performance was degraded. The amplifier could not operate to high enough current to produce the desired peak power output and with the increased RF input power, a very low gain was the end result. The increased bias current caused the amplifier to behave as though it were "current starved." In actuality the cathode was not "current starved" for the peak cathode currents were normal. It was the removal of the space charge by the bias electrode that gave the appearance of current starvation. The bias current was collected at reduced voltage so that there was a net decrease in the power dissipated on the bias electrode; however the degraded overall performance outweighed this achievement.

The results of this experiment did indicate that our understanding of the biased operation is essentially correct, and they also lay the groundwork for the next set of experiments with variations of geometry and electrode location. The next experiment will be to evaluate a bias electrode with a less severe geometry than that used in the successful demonstrations. The results of this next experiment should allow us to partially optimize the electrode configuration and proceed to find the proper location for the electrode for optimum overall performance.

3.0 HIGH POWER AMPLIFIER (SFD-252)

A circular version of the cold test vehicle was constructed complete with input and output waveguides and matching transitions as described in the preceding report. Pole pieces and a dummy cathode were made for the circular cold tester so that it would closely conform to the actual hot test vehicle. A satisfactory match was obtained using the cold test vehicle. The techniques developed were then applied directly to the hot test vehicle. Results on the cold test vehicle match are given along with the preliminary results on the match of the final hot test vehicle. A magnetic circuit tester was made and measurements verified the uniformity of the magnetic field in the interaction space.

3.1 Cold Test - Circular Cold Test Vehicle

The initial circular cold test vehicle had its match adjusted with an absorber on the circuit. The results were shown in the preceding report. The next step was to adjust the match with no absorber on the circuit and with the circuit's output port properly terminated. This technique would show interfering mismatches from both input and output transitions as well as any circuit non-uniformities. The tube is then reversed and the observation is repeated for the other port. A similar technique is used to look at the transmission through the tube, and an indication of insertion loss is observed and recorded. The initial results on the match, both from return loss and insertion loss information, indicated that there was an interfering mode or modes in the tube.

A display of either return loss or transmission loss as a function of frequency will normally show small periodic variations across the band of the tube. The variations in return loss will normally correlate with the variations in transmission loss. The initial results showed these small variations plus other variations which were larger than expected. However, these larger variations did not show correlation

between return loss and transmission loss.

There are several effects which could produce the results observed. The small variations arise from periodic imperfections in the slow wave circuit, e.g., differences in element spacing or the existence of non-uniform braze joints on the circuit. These usually appear and are easily remedied.

The pattern observed in this instance, however, showed pronounced dips in the transmission through the circuit, but without corresponding mismatches as shown in Figure 12. This pattern indicates an absorptive rather than a reflective type of loss. Only a small fraction of the incident power is reflected back through the input, but a significant amount of power is lost in transmission. If we expand a small portion of Figure 12 in the region around 5.0 GHz, we can illustrate this effect. In Figure 13 we show the return loss and transmission loss from Figure 12 and also show the transmission loss which would be produced by the reflections alone. That is, the 6.5 db reflection at 5.0 GHz would normally produce a corresponding 1.1 db of transmission loss. The observed transmission loss is 5 db. (The transmission losses shown in Figure 12 include a 4 db circuit loss which is taken as a reference.) The large transmission loss shows clearly that some energy is being absorbed in the particular geometry of this tester.

The cause was an exchange of energy between the slow wave circuit and the region between the circuit and the back wall of the anode assembly. This effect did not show up in the return loss, as indicated in the preceding report, simply because the absorber on the slow wave circuit damped out this exchange of energy between the back wall and the circuit.

There are several ways in which these effects can be reduced or eliminated. To reduce or eliminate some of the small periodic variations, the elements of the slow wave circuit are carefully checked

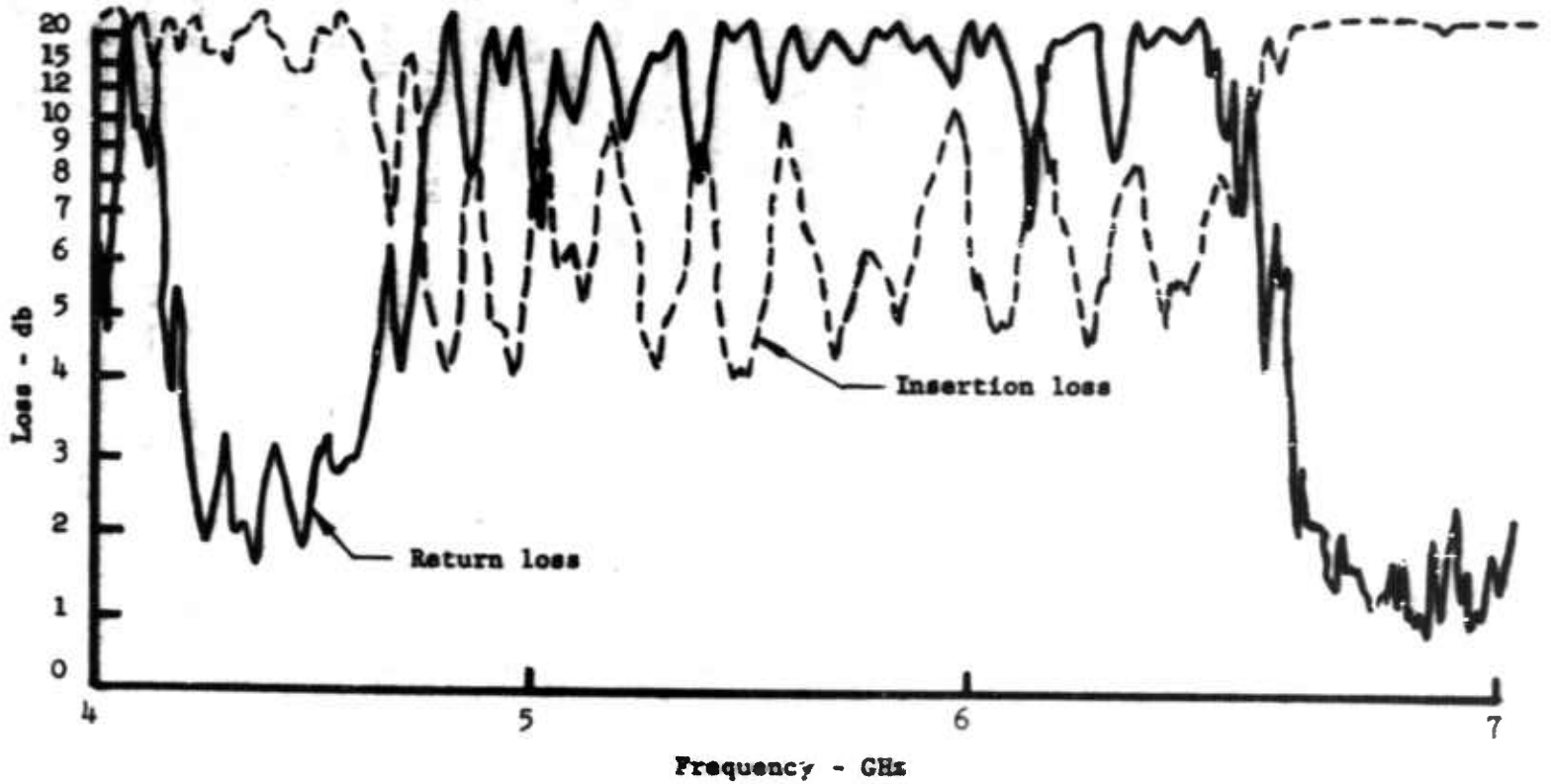

FIGURE 12 TRANSMISSION AND RETURN LOSS FOR CIRCULAR COLD TEST MODEL

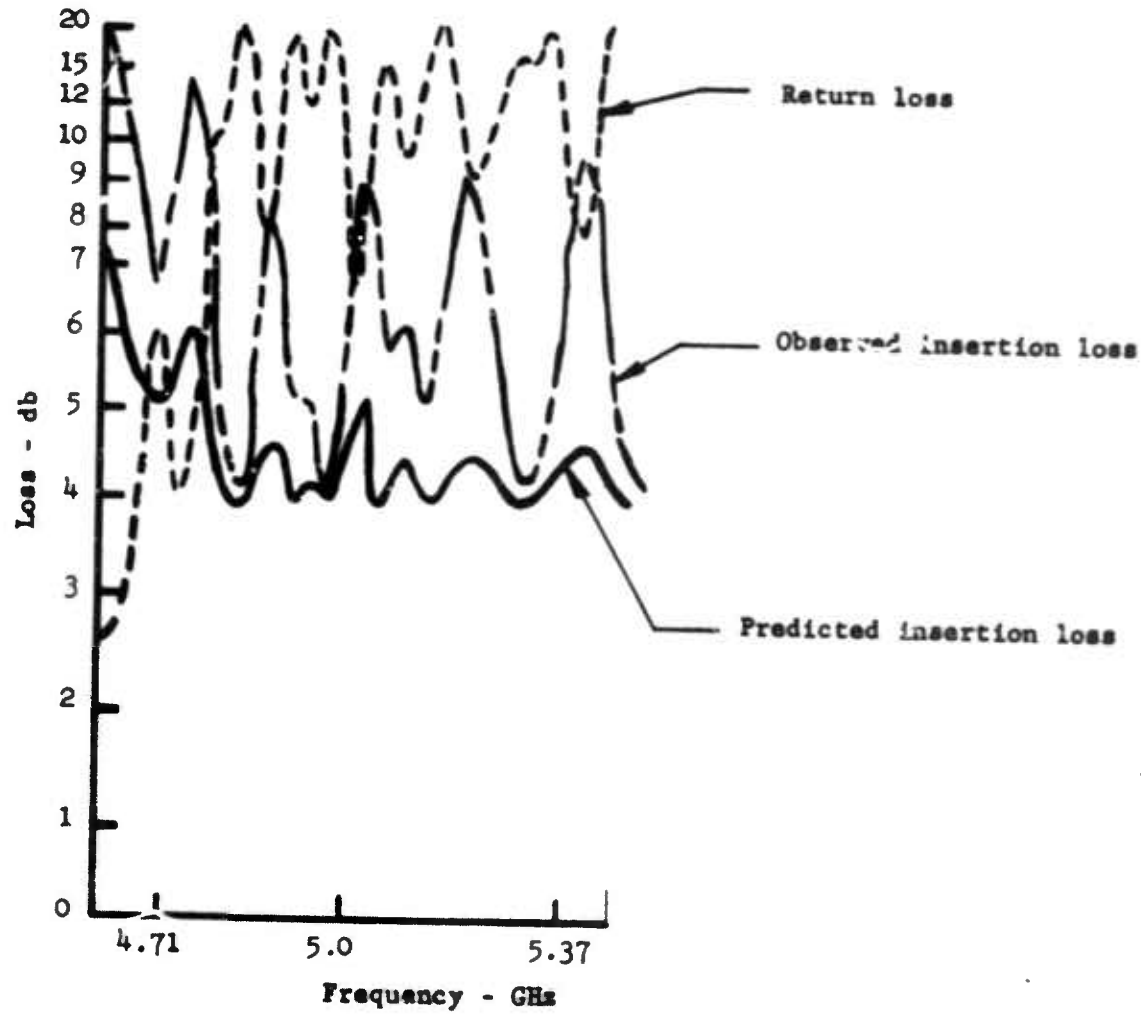

FIGURE 13 EXPANDED VIEW OF INSERTION AND RETURN LOSS FROM FIGURE 12 WITH PREDICTED INSERTION LOSS

and realigned to achieve maximum mechanical uniformity. The more prominent effects with this circuit are the exchange of energy between the slow wave circuit and the back wall region. It was found that the energy propagating between the slow wave circuit and the back wall behaved very much like that which propagates in a ridged waveguide. The method used to reduce or eliminate the coupling between the two propagating systems was to alter the cut-off wavelength of the ridged guide such that its cut-off frequency would fall above the pass band of the slow wave circuit. This was accomplished by altering the geometry of the back wall as shown schematically in Figure 14.

Another effect which has been observed is sometimes difficult to reduce or eliminate. This effect is a cavity resonance. The field must be altered in order to shift the resonance out of the slow wave circuit pass band. The field distribution must be known in order to accomplish this. Again by changing the geometry, the boundary conditions that set up the field can be altered which will shift the resonant frequency.

As a result of these cold tests, changes were made in the geometry of the hot test vehicle. The results will be discussed in the following section.

3.2 Hot Test Vehicle

Techniques for assembling the slow wave circuit evolved through the construction of the cold test model and the initial hot test model. Both of these models had defects in some of the brazed joints formed simultaneously. Efforts to correct these defects by re-brazing resulted in mechanical non-uniformities. The non-uniformities upset the circuit to line match and could not subsequently be corrected. The assembly of the second hot test model was successful. Photographs of this assembly are shown in Figures 15 and 16.

The anode is first brazed into the tube body, after which the cathode and pole pieces are put in place. At this time the match

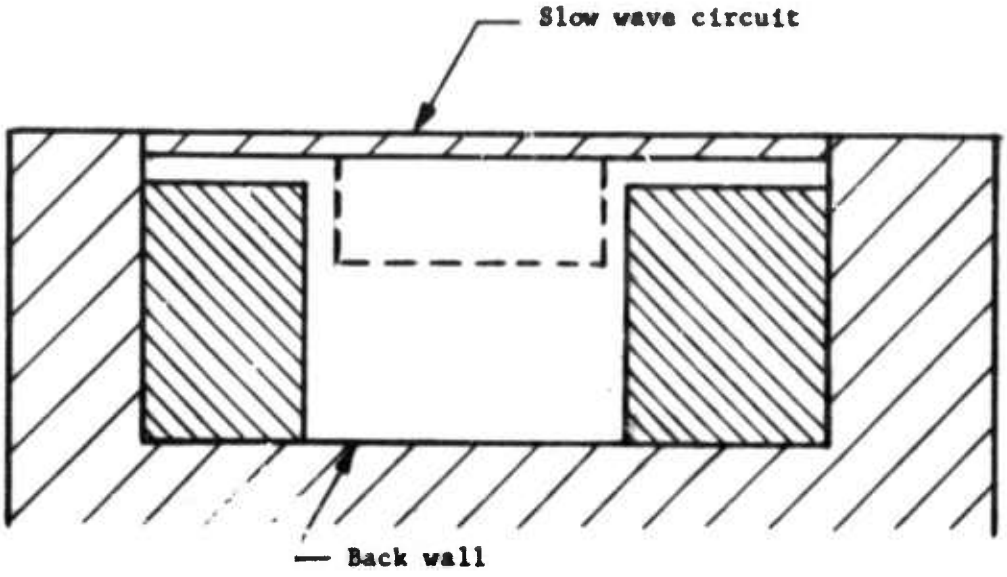

Original geometry of back wall cross-section

New additions to alter back wall cross-section

FIGURE 14 SCHEMATIC OF BACK WALL GEOMETRY SHOWING ALTERATIONS

FIGURE 15 ANODE ASSEMBLY FOR HOT TEST MODEL

FIGURE 16 ANODE FOR HOT TEST MODEL

is observed and recorded as shown in Figures 17 and 18 for return loss, and Figures 19 and 20 for insertion loss. Because of the manner in which the hot test vehicle is assembled, provisions have been made for making final adjustments to the match prior to final seal in of the tube.

The first cathode assembly was found to have a vacuum leak and is being repaired. A second cathode assembly was put together and is now being checked for leaks. Back up piece parts are available for two more anode assemblies and two more cathode assemblies. Once the cathode proves to be leak tight, the complete assembly with pole pieces will be mounted in the tube body. The cathode sub-assembly is shown in Figures 21 and 22.

Figure 23 shows the complete assembly of the hot test vehicle. Three coolant paths are provided in the tube. The anode body has one coolant path with all circuit bars cooled in parallel. This can be seen in Figure 23. The input and output connections for this path are shown at the top of the anode block. The output waveguide, output window, and output transformer make up a second coolant path; The cathode has the third coolant path (not shown). The tubulation seen coming out of the side of the tube body is the pumping port. The ceramic high voltage bushing can be seen (to the left) on the RF input side of the tube.

Figures 24 and 25 are the end view and side view of the hot test vehicle. The coolant system for the cathode and control electrode can be seen. The cathode assembly contains two coolant ports, which also serve as high voltage connections to the cathode and control electrode. The breakway on the upper right of the tube body on Figure 24 shows the general matching scheme. The dashed lines across the output waveguide and the dotted lines, which show the taper into the circuit, constitute the waveguide to coaxial transformer. The output side of the two matching transformers is liquid cooled. The

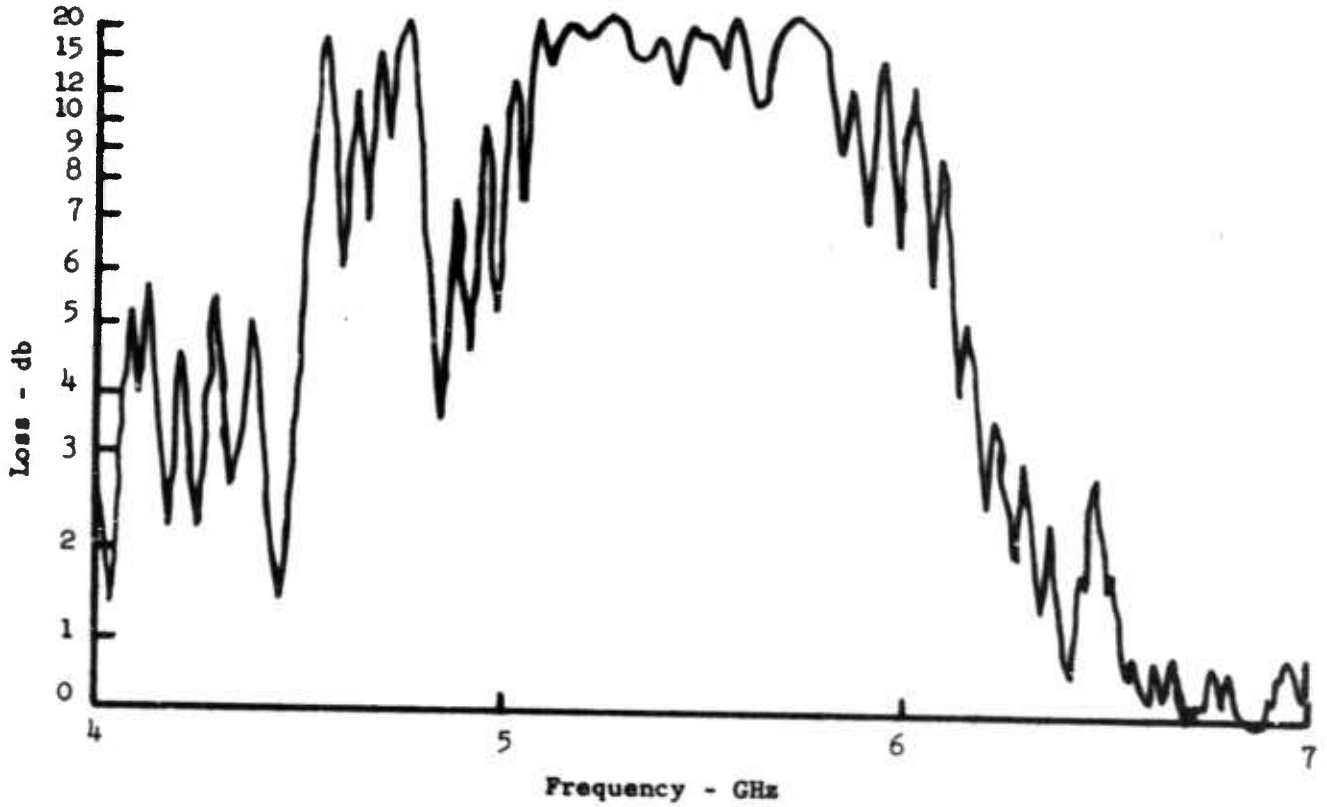

FIGURE 17 INPUT RETURN LOSS FOR HOT TEST VEHICLES

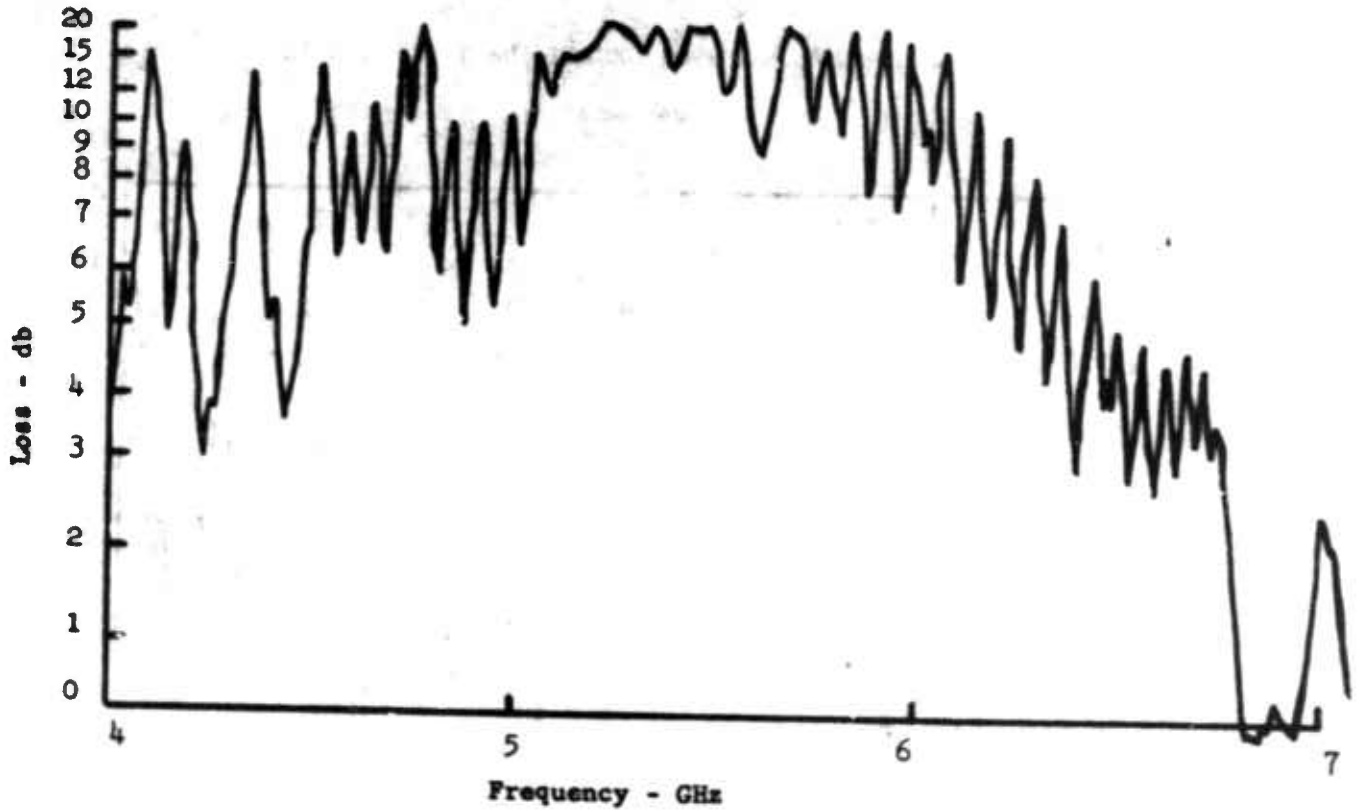

FIGURE 18 OUTPUT RETURN LOSS FOR HOT TEST VEHICLES

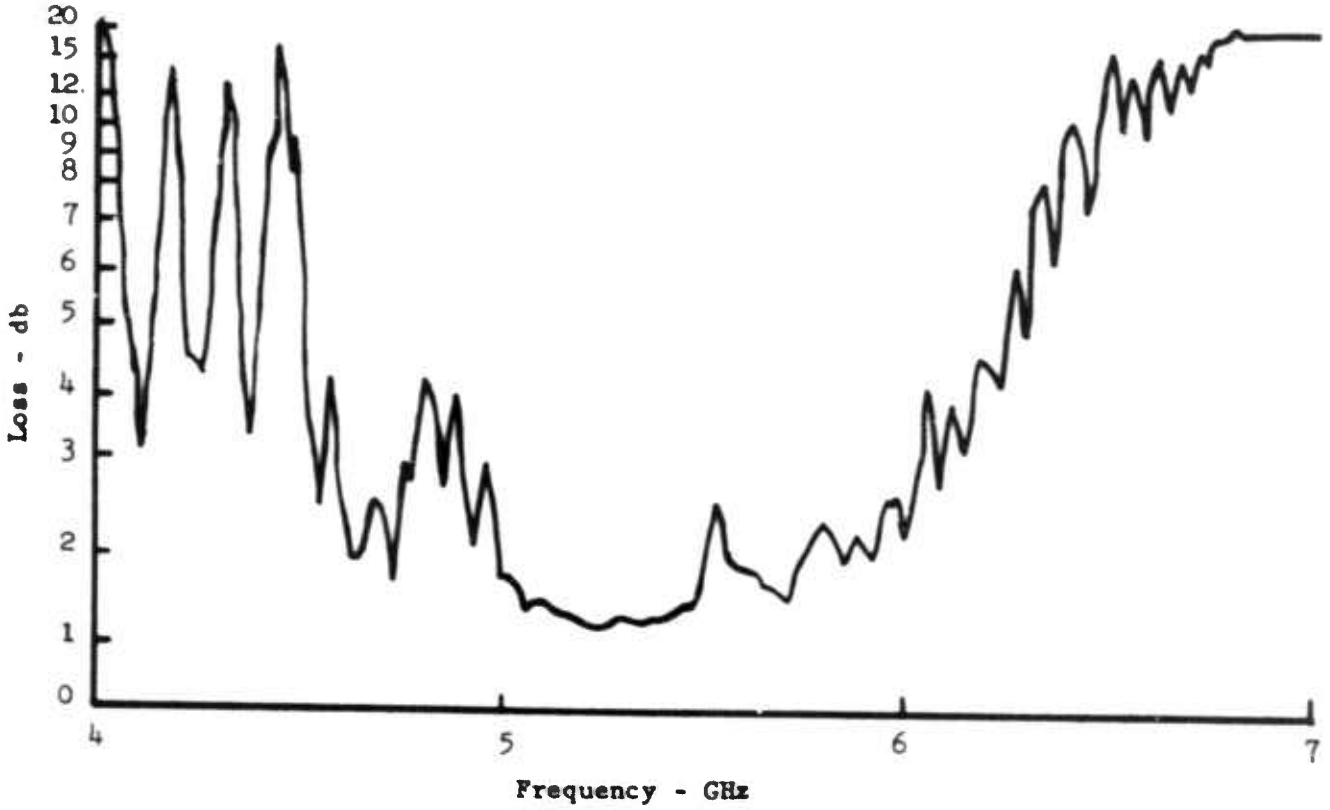

FIGURE 19 INPUT INSERTION LOSS FOR HOT TEST VEHICLE

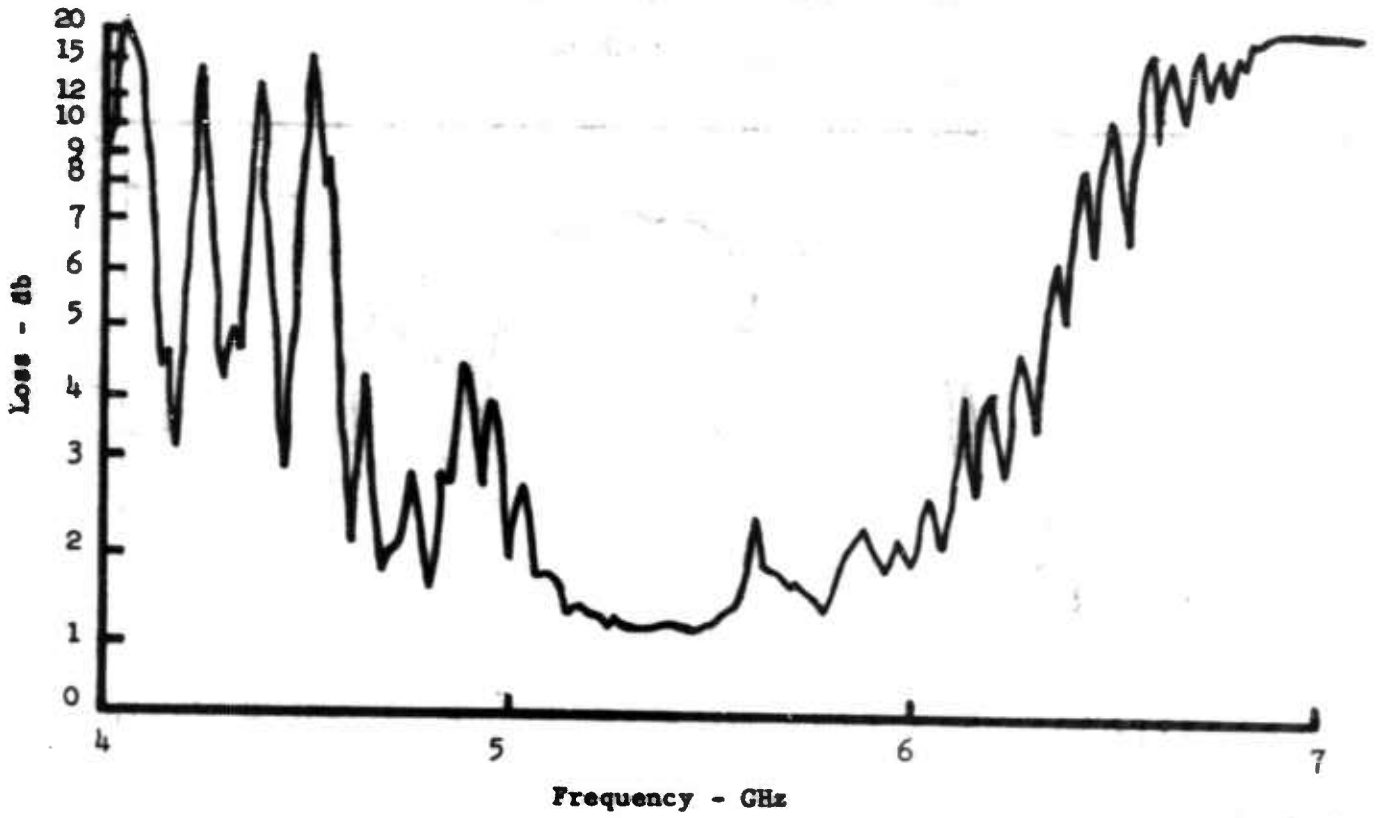

FIGURE 20 OUTPUT INSERTION LOSS FOR HOT TEST VEHICLE

FIGURE 21 CATHODE SUBASSEMBLIES

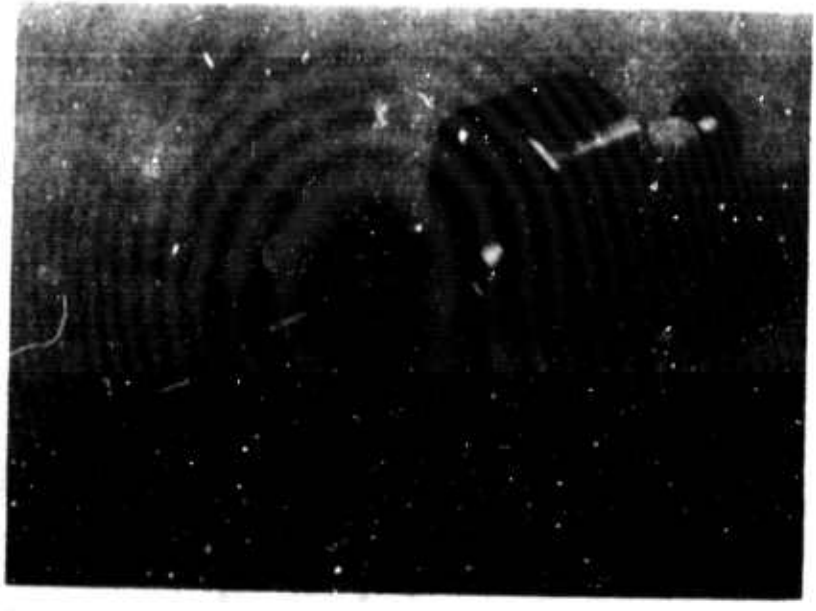

FIGURE 22 CATHODE AND POLE PIECE

FIGURE 23 COMPLETE HOT TEST VEHICLE ASSEMBLY

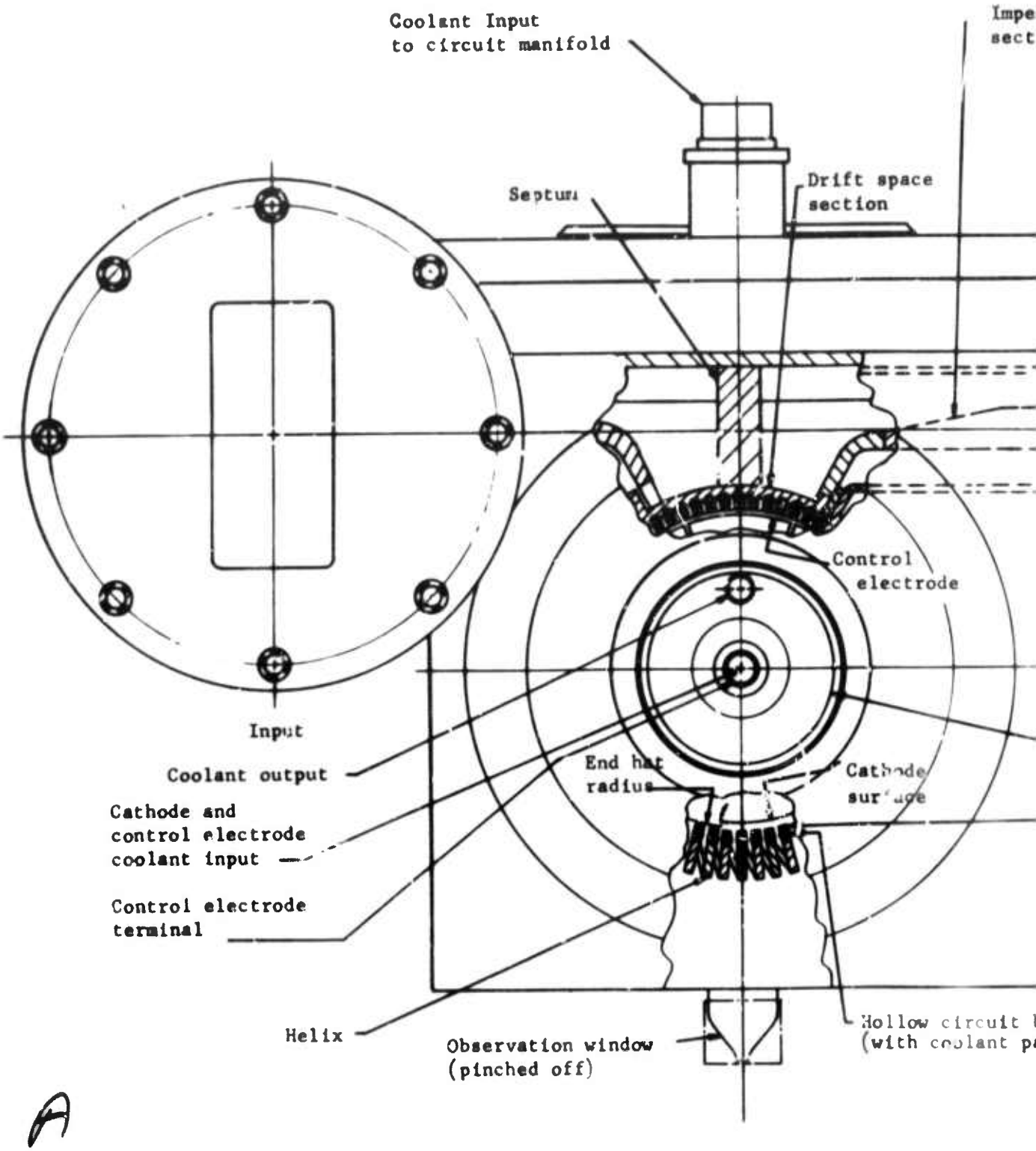

FIGURE 24 END VIEW OF HOT TEST VEHICLE

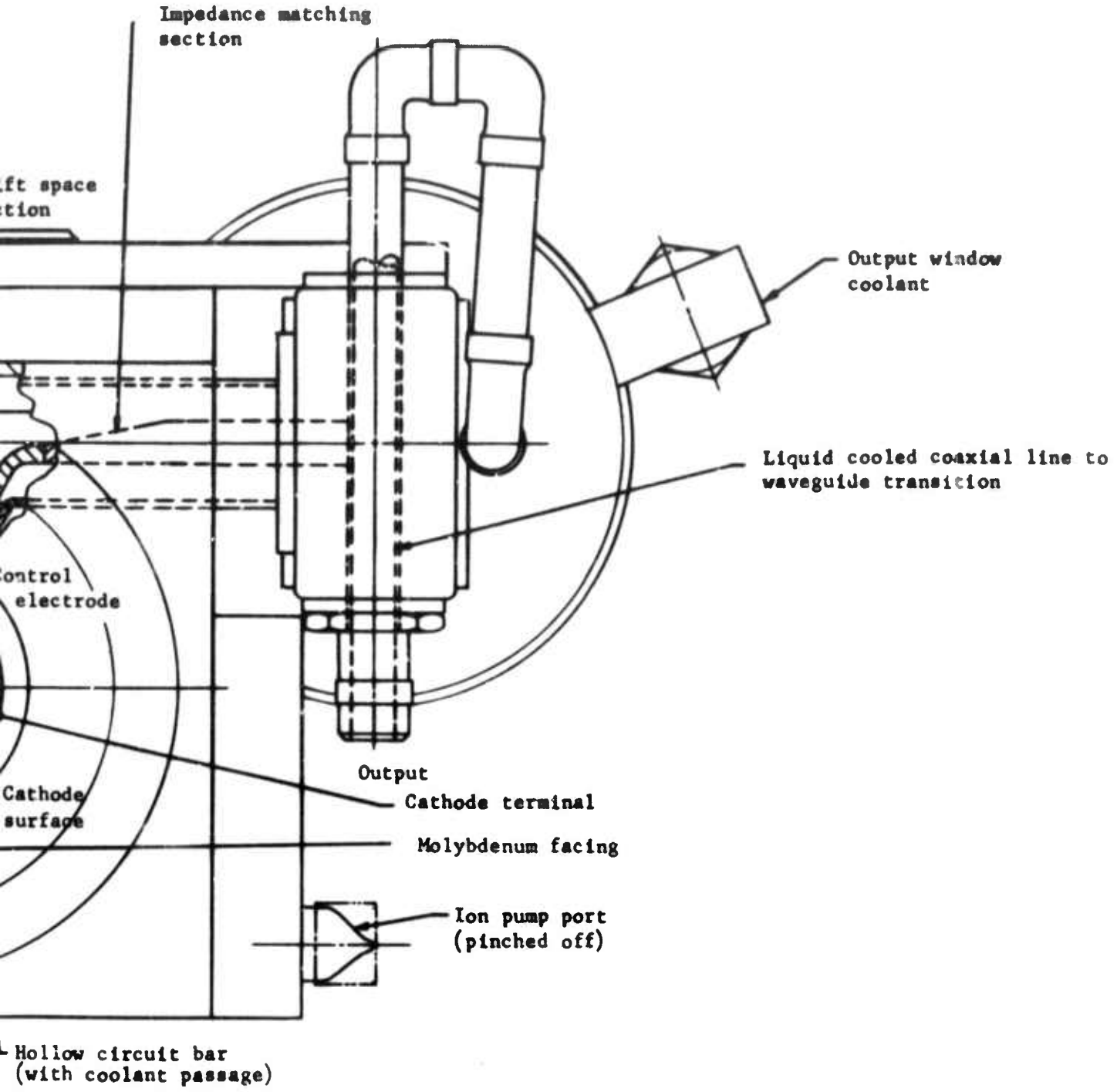
Impedance matching section
ift space
tion
Output window coolant
Liquid cooled coaxial line to waveguide transition
ontrol electrode
Output
Cathode terminal
Cathode surface
Molybdenum facing
Ion pump port (pinched off)
Hollow circuit bar (with coolant passage)

B

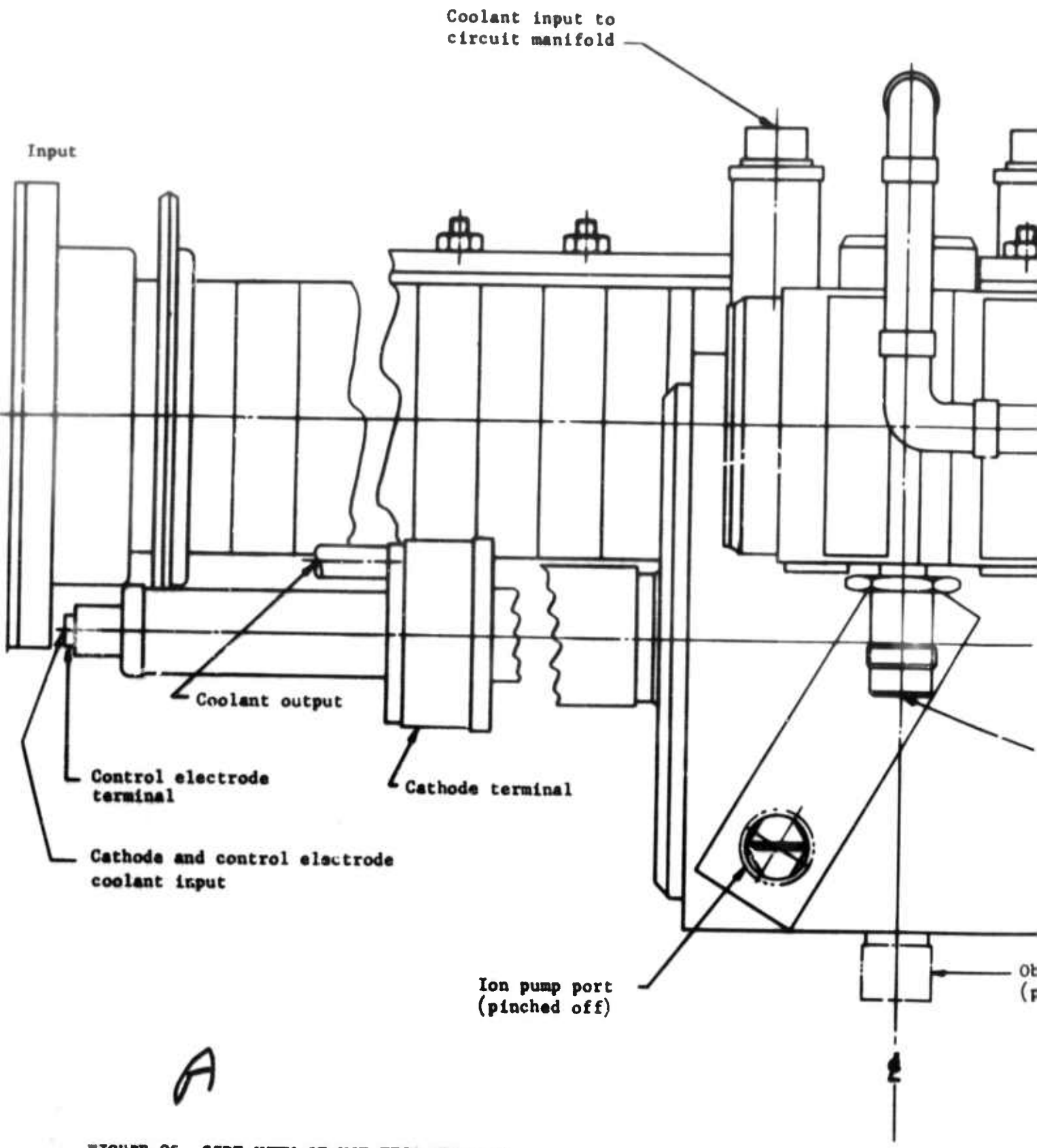

FIGURE 25 SIDE VIEW OF HOT TEST VEHICLE

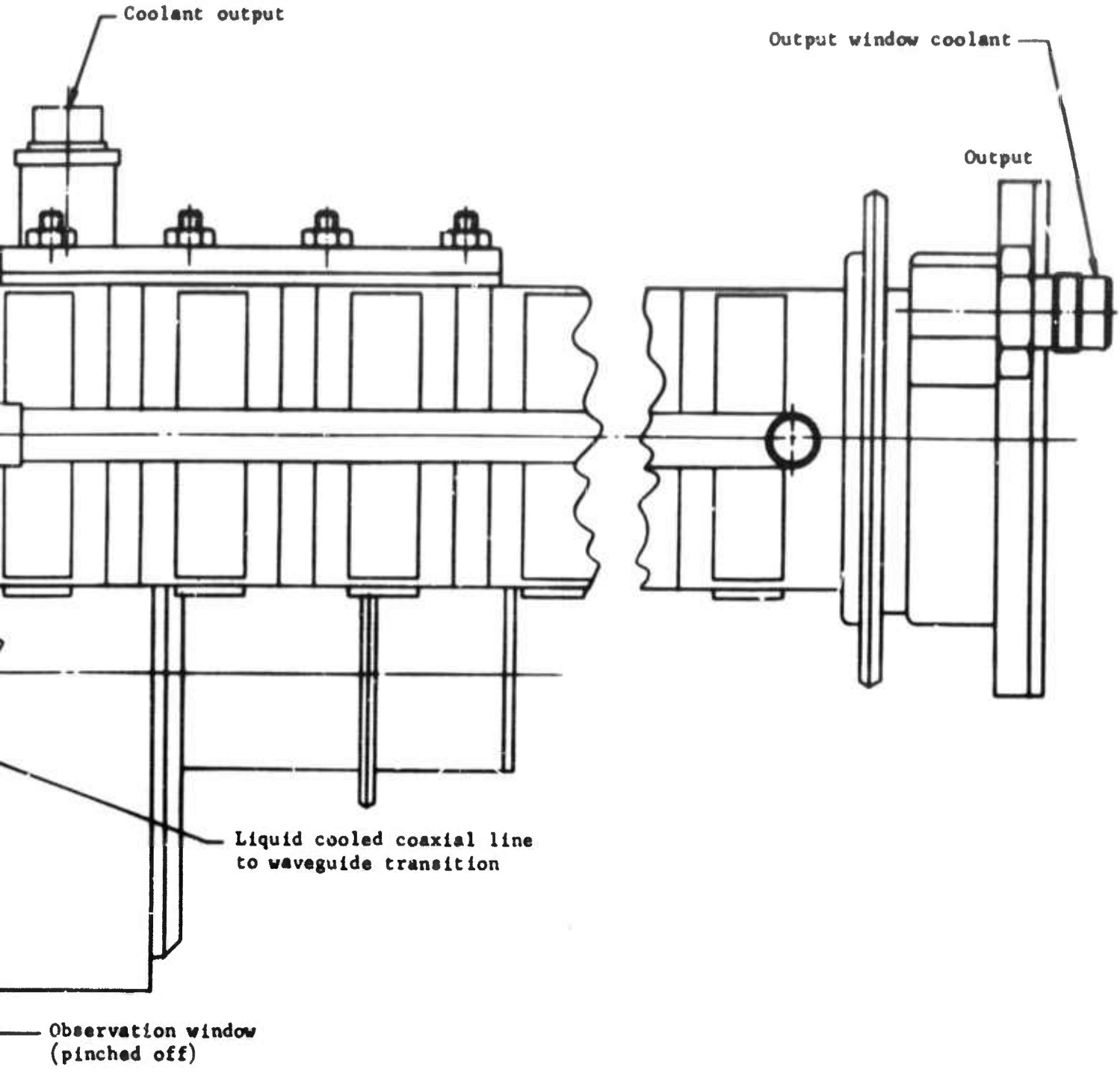
Coolant output
Output window coolant
Output
Liquid cooled coaxial line
to waveguide transition
Observation window
(pinched off)

B

input and output are separated by a septum across the coaxial line above the drift space section. An observation port is provided at the bottom of the body of the hot test vehicle so that a small part of the circuit and cathode surface can be seen during operation.

The hot test vehicle should be completed toward the latter part of June 1968.

3.3 Magnetic Circuit

Parts for a magnetic cold tester were completed with provision to measure the flux density in the interaction space. The cold test magnetic circuit is shown in Figure 26.

The pole pieces were shaped in order to provide a fairly uniform flux density in the interaction space. This was verified by the measurements taken. The results of these measurements are shown in the flux density field plot in Figure 27. As can be seen, the field is fairly uniform in the shaded area which represents the interaction space.

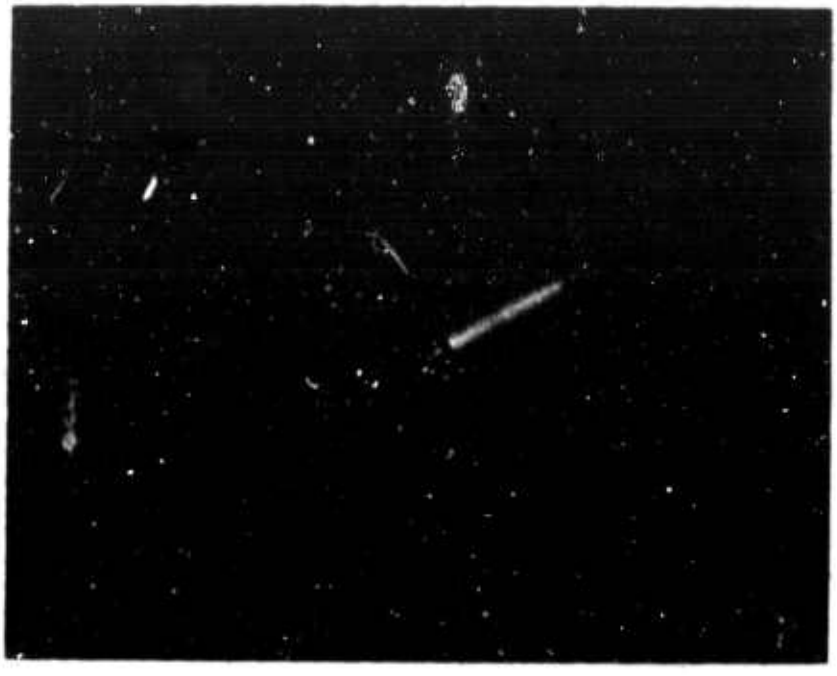

FIGURE 26 MAGNETIC CIRCUIT COLD TESTER

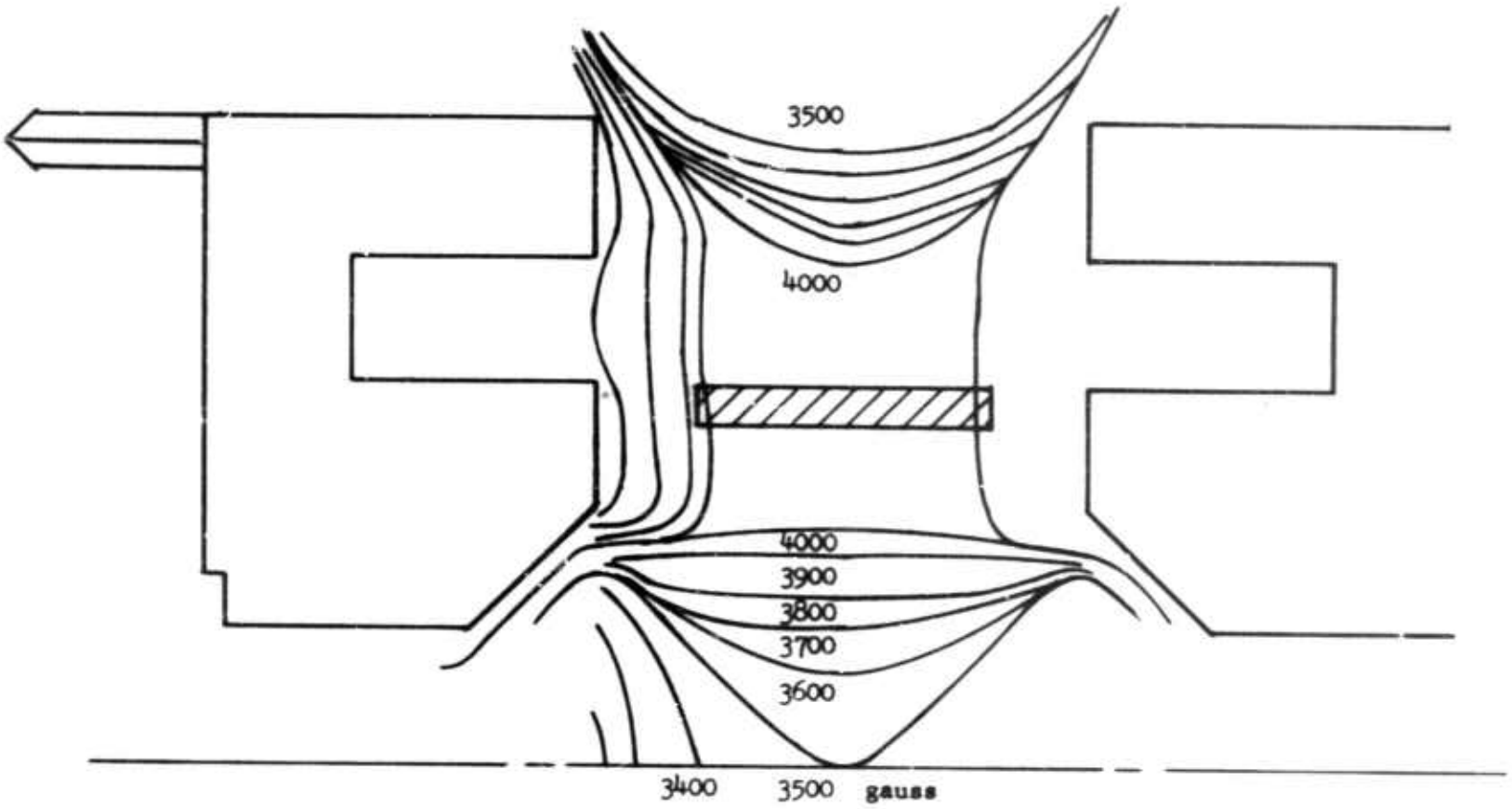

FIGURE 27 FIELD PLOT OF MAGNETIC FLUX DENSITIES USING MAGNETIC COLD TESTER

4.0 PROGRAM FOR NEXT PERIOD

1. Complete construction of the hot test vehicle.
2. Begin hot test evaluation of high power operation.
3. Continue tests to evaluate and optimize the self-turn off operation.

Unclassified

Security Classification

DOCUMENT CONTROL DATA - R & D

(Security classification of title, body of abstract and indexing annotation must be entered when the overall report is classified)

1. ORIGINATING ACTIVITY (Corporate author)
S-F-D laboratories, inc.
800 Rahway Avenue
Union, New Jersey 07083

2a. REPORT SECURITY CLASSIFICATION
Unclassified

2b. GROUP
--

3. REPORT TITLE
C-BAND PHASED ARRAY CROSSED-FIELD AMPLIFIER DEVELOPMENT

4. DESCRIPTIVE NOTES (Type of report and inclusive dates)
Quarterly Report No. 3, Feb 1968 - May 1968

5. AUTHOR(S) (First name, middle initial, last name)
R. Bitzer; A. Wilczek

6. REPORT DATE
August 1968

7a. TOTAL NO. OF PAGES
45

7b. NO. OF REFS
0

8a. CONTRACT OR GRANT NO.
F30602-68-C-0055

b. PROJECT NO.
ARPA Order 136

c. Amendment No. 15

d.

9a. ORIGINATOR'S REPORT NUMBER(S)
118-R-3

9b. OTHER REPORT NO(S) (Any other numbers that may be assigned this report)
RADC-TR-68

10. DISTRIBUTION STATEMENT
This document is subject to special export controls and each transmittal to foreign governments, foreign nationals or representatives thereto may be made only with prior approval of RADC (EMATE), Griffiss AFB, New York, 13440

11. SUPPLEMENTARY NOTES
Project Engineer, Capt. R.L. DuBois, RADC (EMATE), Griffiss Air Force Base New York 13440

12. SPONSORING MILITARY ACTIVITY
Advanced Research Projects Agency, Washington, D.C.

13. ABSTRACT

This program has two main objectives. The first is to demonstrate the feasibility of an RF turn-on, RF turn-off, reentrant stream crossed-field amplifier. The reliability of RF turn-on has previously been demonstrated and during this reporting period, RF turn-off has been demonstrated with only dc voltages applied to the amplifier.

The second objective of this program is to increase the output capability previously demonstrated, ~~under Contract AF 30(602)-4088,~~ by a factor of two. During this period a hot test vehicle has been successfully assembled and the matching transitions have been developed.

DD FORM 1473

Unclassified

Security Classification